

# Compatible finite element methods for numerical weather prediction

C. J. Cotter and A. T. T. McRae

*Imperial College,  
London, UK*

## ABSTRACT

This article takes the form of a tutorial on the use of a particular class of mixed finite element methods, which can be thought of as the finite element extension of the C-grid staggered finite difference method. The class is often referred to as compatible finite elements, mimetic finite elements, discrete differential forms or finite element exterior calculus. We provide an elementary introduction in the case of the one-dimensional wave equation, before summarising recent results in applications to the rotating shallow water equations on the sphere, before taking an outlook towards applications in three-dimensional compressible dynamical cores.

## 1 Introduction

Mixed finite element methods are a generalisation of staggered finite difference methods, and are intended to address the same problem: spurious pressure mode(s) observed in the finite difference A-grid and are also observed in finite element methods when the same finite element method, different finite element spaces are selected for different variables. The vast range of available finite element spaces is both a blessing and a curse, and many different combinations have been proposed, analysed and used for large scale geophysical fluid dynamics applications, particularly in the ocean modelling community [Le Roux et al. \(2005, 2007\)](#); [Le Roux and Pouliot \(2008\)](#); [Danilov \(2010\)](#); [Cotter et al. \(2009\)](#); [Cotter and Ham \(2011\)](#); [Rostand and Le Roux \(2008\)](#); [Le Roux \(2012\)](#); [Comblen et al. \(2010\)](#), whilst many other combinations have been used in engineering applications where different scales and modelling aspects are important.

In this article we limit the scope considerably by discussing only one particular family of mixed finite element methods, known variously as compatible finite elements (the term that we shall use here), mimetic finite elements, discrete differential forms or finite element exterior calculus. These finite element methods have the important property that differential operators such as grad and curl map from one finite element space; these embedding properties lead to discrete versions of the div-curl and curl-grad identities of vector calculus. This echoes the important “mimetic” properties of the C-grid finite difference method, discussed in full generality on unstructured grids, and shown to be highly relevant and useful in geophysical fluid dynamics applications, in [Thuburn et al. \(2009\)](#); [Ringler et al. \(2010\)](#). This generalisation of the C-grid method is very useful since it allows (i) use arbitrary grids, with no requirement of orthogonal grids, without loss of consistency/convergence rate; (ii) extra flexibility in the choice of discretisation to optimize the ratio between global velocity degrees of freedom (DoFs) and global pressure DoFs to eliminate spurious mode branches; and (iii) the option to increase the consistency/convergence order.

Compatible finite element methods were first identified in the 1970s, and quickly became very popular amongst numerical analysts since this additional mathematical structure facilitated proofs of stability and convergence, and provided powerful insight. These results were collected and unified in [Brezzi and Fortin \(1991\)](#), an excellent book which has been out of print for a long time, but a new addition

has recently appeared [Boffi et al. \(2013\)](#). These methods have become the standard tool for ground-water modelling using Darcy’s law [Allen et al. \(1985\)](#), and have also become very popular for solving Maxwell’s equations [Bossavit \(1988\)](#); [Hiptmair \(2002\)](#) where a mathematical structure based on differential forms was developed by Bossavit, together with the term “discrete differential forms”. This structure was enriched, extended and unified under the term “finite element exterior calculus” by Douglas Arnold and collaborators [Arnold et al. \(2006, 2010\)](#), who used the framework to develop new stable discretisations for elasticity. This has produced a rich and beautiful theory in the language of exterior calculus, however, in this article we shall only use standard vector calculus notation.

In geophysical applications, the stability properties of compatible finite elements have long been recognised, leading to various choices being proposed and analysed on triangular meshes [Walters and Casulli \(1998\)](#); [Rostand and Le Roux \(2008\)](#). However, no explicit use was made of the compatible structure beyond stability until [Cotter and Shipton \(2012\)](#), which proved that all compatible finite element methods have exactly steady geostrophic modes; this is considered a crucial property for numerical weather prediction [Staniforth and Thuburn \(2012\)](#). They also showed that the global DoF balance between velocity and pressure in compatible finite element discretisations is crucial in determining the existence of spurious mode branches. If there are less than 2 velocity DoFs of freedom per pressure DoF, then there will be branches of spurious inertia-gravity wave branches. This occurs in the RT0-DG0 (lowest order Raviart-Thomas space for velocity, and piecewise constant for pressure) on triangles, as demonstrated by Danilov in [Danilov \(2010\)](#). In fact, if the Rossby radius is not resolved<sup>1</sup>, then the spurious and physical branches merge leading to disastrous results. On the other hand, if the velocity/pressure global DoF ratio is greater than 2:1, there will be spurious Rossby modes similar to those observed for the hexagonal C-grid [Thuburn \(2008\)](#). [Cotter and Shipton \(2012\)](#) identified the BDFM1-DG1 spaces (1st Brezzi-Douglas-Fortin-Marini space for velocity, linear discontinuous space for pressure) on triangles, and the RTk-DG1 ( $k$ th Raviart-Thomas space for velocity,  $k$ th order discontinuous space for pressure) on quadrilaterals as having potential for numerical weather prediction, due to their exact global 2:1 DoF ratio.

Recently, there has been some further developments in the application of compatible finite element methods to the nonlinear rotating shallow water equations on the sphere, as part of the UK Dynamical Core “Gung Ho” project. An efficient software implementation of the compatible finite element spaces on the sphere was provided in [Rognes et al. \(2014\)](#), whilst an energy-entropy conserving formulation analogous to the energy-entropy conserving C-grid formulation of [Arakawa and Lamb \(1981\)](#) was provided in [McRae and Cotter \(pear\)](#). A discussion of these properties in the language of finite element exterior calculus was provided in [Cotter and Thuburn \(2014\)](#).

In this article we provide an elementary introduction to compatible finite element methods, for a reader equipped with knowledge of vector calculus, and calculus of variations. We begin with a simple linear one-dimensional example in Section 2. We then discuss applications to the linear and nonlinear shallow-water equations in Section 3. Finally, we provide a glimpse of current work developing three dimensional formulations for numerical weather prediction in Section 4.

## 2 One dimensional formulation

In this section we develop the compatible finite element method in the context of the one-dimensional scalar wave equation on the domain  $[0, L]$  with periodic boundary conditions,

$$h_{tt} - h_{xx} = 0, \quad h(0, t) = h(L, t). \quad (1)$$

<sup>1</sup>The barotropic Rossby radius is rarely resolved in ocean models, and the higher baroclinic Rossby radii (there are  $n - 1$  of these in an  $n$ -layer model) get smaller and smaller. This means that there are unresolved Rossby radii in all numerical weather prediction models.

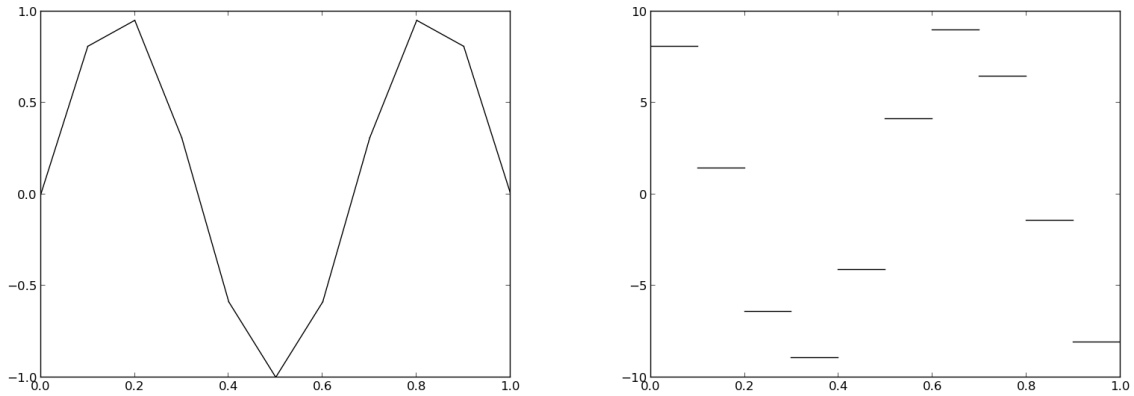


Figure 1: Example finite element functions for a subdivision of the domain  $[0, 1]$  into 10 elements. Left: A function from the CG1 finite element space. Right: A function from the DG0 finite element space.

It is more relevant to issues arising in the shallow water equations, and beyond, to split this equation into two first order equations, in the form

$$u_t + h_x = 0, \quad h_t + u_x = 0, \quad h(0, t) = h(L, t), \quad u(0, t) = u(L, t). \quad (2)$$

In this section, we shall discretise Equation (2) in space using compatible finite element methods.

In general, the finite element method is based on two key ideas: (i) the approximation of the numerical solution by functions from some chosen finite element spaces, and (ii) the weak form. We shall motivate the latter by discussing the former in the context of Equation (2).

**Definition 1** (Finite element space (on a one-dimensional domain)). *We partition the interval  $[0, L]$  into  $N_e$  non-overlapping subintervals, which we call elements; the partition is called a mesh. We shall call the point shared by two neighbouring elements a vertex. A finite element space is a collection of functions on  $[0, L]$  which are:*

1. *polynomials of some specified maximum degree  $p$  when restricted to each element  $e$ , and*
2. *have some specified degree of continuity (discontinuous, continuous, continuous derivative, etc.)*

The most common options for continuity are continuous functions, in which case we name the finite element space  $CG(p)$  for given  $p$ , and discontinuous functions, in which case we name the finite element space  $DG(p)$  (higher order continuity finite element spaces are more exotic, B-splines for example, and we shall not discuss them here). An example function from the CG1 space and an example function from the DG0 space are shown in Figure 1. We use the term finite element space since the collection of functions form a vector space (*i.e.*, they may be added together and scaled by real numbers, and addition and scaling satisfy the required properties of a vector space). This makes finite element spaces amenable to the tools of linear algebra. We also note that finite element spaces are finite dimensional. This makes them amenable to calculation on a computer.

We now proceed to discretise Equation (2). We would like to restrict both  $h$  and  $u$  to finite element spaces, let us say CG1 for the purposes of this discussion (we will use the notation  $u \in CG1$  to mean that  $u$  is a function in the finite element space CG1). Clearly we do not obtain solutions of (2), since if  $u \in CG1$  then  $u_x \in DG0$ . (In fact, we obtained the DG0 function in Figure 1 by taking the derivative of

the CG1 function.) Hence, we choose to find the best possible approximation to (2) by minimising the magnitude of  $u_t + h_x$  and  $h_t + u_x$  whilst keeping  $u$  and  $h$  in CG 1. To do this, we need to choose a way of measuring the magnitude of functions (*i.e.*, a norm), of which the  $L^2$  norm, given by

$$\|u\|_{L^2} = \sqrt{\int_0^L u^2 dx}, \quad (3)$$

is the most natural and computationally feasible. Our finite element approximation becomes<sup>2</sup>

$$\min_{u_t \in \text{CG1}} \frac{1}{2} \|u_t + h_x\|^2, \quad \min_{h_t \in \text{CG1}} \frac{1}{2} \|h_t + u_x\|^2. \quad (4)$$

The standard calculus of variations approach to finding the minimiser  $u_t$  for the first of Equations (4) follows from noting if  $u_t$  is optimal, then infinitesimal changes in  $u_t$  do not change the value of  $\|u_t + h_x\|^2$ . This is expressed mathematically as

$$\lim_{\varepsilon \rightarrow 0} \frac{\frac{1}{2} \|u_t + \varepsilon w + h_x\|^2 - \frac{1}{2} \|u_t + h_x\|^2}{\varepsilon}, \quad (5)$$

for any  $w \in \text{CG1}$  (we adopt the notation  $\forall w \in \text{CG1}$ ). We obtain

$$\begin{aligned} 0 &= \lim_{\varepsilon \rightarrow 0} \frac{1}{2} \|u_t + \varepsilon w + h_x\|^2 - \frac{1}{2} \|u_t + h_x\|^2, \\ &= \frac{1}{2} \int_0^L (u_t + \varepsilon w + h_x)^2 dx - \frac{1}{2} \int_0^L (u_t + h_x)^2 dx, \\ &= \frac{1}{2} \int_0^L (u_t + h_x)^2 + 2\varepsilon w(u_t + h_x) dx - \frac{1}{2} \int_0^L (u_t + h_x)^2 dx, \\ &= \int_0^L w(u_t + h_x) dx, \quad \forall w \in \text{CG1}. \end{aligned} \quad (6)$$

An identical calculation follows for the  $h_t$  equation, and we obtain

$$0 = \int_0^L \phi(u_t + h_x) dx, \quad \forall \phi \in \text{CG1}. \quad (7)$$

We refer to  $w$  and  $\phi$  as *test functions*. Note that Equations (6-7) can be directly obtained by multiplying Equations (2) by test functions  $w$  and  $\phi$ , and integrating over the domain; the minimisation process is only a theoretical tool to explain that it is the best possible approximation using the finite element space. Since these equations represent the error-minimising approximations of Equations (2) with  $u \in \text{CG1}$ ,  $p \in \text{CG1}$ , we call them the *projections* of Equations (2) onto CG1. In general, the projection of an function or an equation onto a finite element space is called *Galerkin projection*.

Equations (6-7) can be implemented efficiently on a computer by expanding  $w$ ,  $\phi$ ,  $u$  and  $h$  in a basis over CG1,

$$u(x) = \sum_{i=1}^n N_i(x) u_i, \quad h(x) = \sum_{i=1}^n N_i(x) h_i, \quad w(x) = \sum_{i=1}^n N_i(x) w_i, \quad \phi(x) = \sum_{i=1}^n N_i(x) \phi_i, \quad (8)$$

with real valued basis coefficients  $u_i$ ,  $w_i$ ,  $h_i$ ,  $\phi_i$ . These basis coefficients are still functions of time since we have not discretised in time yet. In general, in one dimension it is always possible to find a basis for CG( $p$ ) and DG( $p$ ) finite element spaces such that the basis functions  $N_i$  are non-zero in at most two (neighbouring) elements. For details of the construction of basis functions for CG and DG spaces of arbitrary  $p$ , see [Karniadakis and Sherwin \(2005\)](#). Substitution of these basis expansions into Equations (6-7) gives

$$w^T (M\dot{u} + Dh) = 0, \quad \phi^T (M\dot{h} + Du) = 0, \quad (9)$$

<sup>2</sup>The factors of 1/2 are not significant but they simplify the subsequent equations.

where  $M$  and  $D$  are matrices with entries given by

$$M_{ij} = \int_0^L N_i(x)N_j(x) dx, \quad D_{ij} = \int_0^L N_i(x)\frac{\partial N_j}{\partial x}(x) dx, \quad (10)$$

and  $u$ ,  $h$ ,  $w$  and  $\phi$  are vectors of basis coefficients with  $u = (u_1, u_2, \dots, u_n)$  etc. Equations (9) must hold for all test functions  $w$  and  $\phi$ , and therefore for arbitrary coefficient vectors  $w$  and  $\phi$ . Therefore, we obtain the matrix-vector systems,

$$M\dot{u} + Dh = 0, \quad M\dot{h} + Du = 0. \quad (11)$$

Having chosen a basis where each basis function vanishes in all but two elements, the matrices  $M$  and  $D$  are extremely sparse and hence can be assembled efficiently. For details of the efficient assembly process, see [Karniadakis and Sherwin \(2005\)](#). Furthermore, the matrix  $M$  is well-conditioned and hence can be cheaply inverted using iterative methods [Wathen \(1987\)](#). It remains to integrate Equations (11) using a discretisation in time. A generalisation of this approach is used for all of the finite element methods that we describe in this paper.

One key problem with Equations (6-7) is that of spurious modes. For example, if we use a regular grid of  $N_e$  elements of the same size, if  $h$  is a CG1 “zigzag” function that alternates between 1 and  $-1$  between each vertex, then  $h_x$  is a DG0 “flip-flop” function that takes the value  $\Delta x$  and  $-\Delta x$  in alternate elements, where  $\Delta x = N_e/L$ . Multiplication by a CG1 test function  $w$  and integrating then gives zero for arbitrary  $w$ . The easiest way to understand why is to choose  $w$  to be a hat-shaped basis function that is equal to 1 at a single vertex, and 0 at all other vertices. Then the integral of  $w$  multiplied by  $h_x$  is a (scaled) average of  $h_x$  over two elements, which is equal to zero. Since all  $w$  can be expanded in basis functions of this form, we obtain  $Dw$  in every case. This is a problem because our original zigzag function is very oscillatory, and so the approximation of the derivative should be large. In general, using the same finite element space for  $u$  and  $h$  leads to the existence of spurious modes which have very small numerical derivatives, despite being very oscillatory, and hence propagate very slowly. When nonlinear terms are introduced, these modes get coupled to the smooth part of the function, and grow rapidly, making the numerical scheme unusable.

In finite difference methods, this problem is avoided by using staggered grids, with different grid locations for  $u$  and  $h$ . In finite element methods, the analogous strategy is to choose different finite element spaces for  $u$  and  $h$ . This is referred to as a *mixed finite element method*. We shall write  $u \in V_0$ ,  $h \in V_1$  and discuss different choices for  $V_0$  and  $V_1$ . In particular, we shall choose  $V_0 = \text{CG1}$  and  $V_1 = \text{DG0}$ , together with the higher-order extensions  $V_0 = \text{CG}(p)$  and  $V_1 = \text{DG}(p-1)$ , for some chosen  $p > 1$ . The reason for doing this is that if  $u \in V_0$ , then  $u_x \in V_1$ : this is because  $u$  is continuous but can have jumps in the derivative, and differentiation reduces the degree of a polynomial by 1. We say that the finite element spaces  $V_0$  and  $V_1$  are *compatible* with the  $x$ -derivative. This choice means that  $h_t + u_x \in V_1$  and there is no approximation in writing that equation. Put another way, the Galerkin projection in Equation 7 is “trivial”, *i.e.* it does not change the equation.

To write down our compatible finite element method we have one further issue to address, namely that  $h \in V_1$  is discontinuous, and so  $h_x$  is not globally defined. This is dealt with by integrating the  $h_x$  term by parts in the finite element approximation, and we obtain

$$\begin{aligned} \int_0^L w u_t - w_x h dx &= 0, \quad \forall w \in V_0, \\ \int_0^L \phi (h_t + u_x) dx &= 0, \quad \forall \phi \in V_1. \end{aligned}$$

There is no boundary term arising from integration by parts due to the periodic boundary conditions. Three out of the four terms in these two equations involve trivial projections that do nothing, the  $u_t$ ,  $h_t$  and  $u_x$  terms. This means that they introduce no further errors beyond approximating the initial

conditions in the finite element spaces. The only term that we have to worry about is the discretised  $h_x$  term, where we would like to convince ourselves that there are no spurious modes. This is done by showing that the following mathematical condition holds.

**Definition 2** (inf-sup condition). *The spaces  $V_0$  and  $V_1$  satisfy the inf-sup condition<sup>3</sup> if there exists a constant  $C > 0$ , independent of the choice of mesh, such that*

$$\sup_{w \in V_0, w \neq 0} \frac{\left| \int_0^L w_x h dx \right|}{\|w_x\|_{L^2}} \geq C \|h\|_{L^2}, \tag{12}$$

for all non-constant  $h \in V_1$ .

This prevents spurious modes because it says that for any non-constant  $h$ , there exists at least one  $w$  such that the integral is reasonably large in magnitude compared to the size of  $w_x$  and  $h$ . In general, proving the inf-sup condition for mixed finite element methods is a fairly technical business (see [Auricchio et al. \(2004\)](#) for a review). However, for our compatible finite element discretisation it is completely straightforward.

**Proposition 3** (inf-sup condition for compatible finite elements). *Let  $V_0$  and  $V_1$  be chosen such that if  $h \in V_1$  is non-constant then we can find  $w \in V_0$  such that  $w_x = h$ . Then the inf-sup condition is satisfied, with  $C = 1$ .*

*Proof.* For any non-constant  $h$ , take  $w'$  such that  $w'_x = h$  (which is possible by the assumption of the proposition). Then

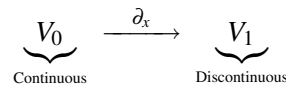
$$\sup_{w \in V_0} \frac{\left| \int_0^L w_x h dx \right|}{\|w_x\|_{L^2}} \geq \frac{\left| \int_0^L w'_x h dx \right|}{\|w'_x\|_{L^2}} = \frac{\|h\|_{L^2}^2}{\|h\|_{L^2}} = \|h\|_{L^2}. \tag{13}$$

□

The assumption of the proposition is true whenever  $V_0 = \text{CG}(p)$ ,  $V_1 = \text{DG}(p - 1)$ . This means that our compatible finite element methods will be free from spurious modes. This concludes our discussion of the one-dimensional case; in the next section we discuss the construction of two-dimensional compatible finite element spaces and their application to the shallow water equations.

### 3 Application to linear and nonlinear shallow water equations on the sphere

In one dimension, a compatible finite element method was described for the wave equation, by choosing two finite element spaces  $V_0$  and  $V_1$ , such that (i) if  $u \in V_0$ , then  $u_x \in V_1$ ; and (ii) if  $p \in V_1$  then there is  $u \in V_0$  such that  $u_x = p$ . We represent this structure by the following diagram.



Recall that functions in  $V_0$  are continuous, which allows the derivative to be globally defined.

In two dimensions, we take our computational domain, denoted  $\Omega$ , to be a rectangle in the plane with periodic boundary conditions<sup>4</sup>, and partition it into either triangular or quadrilateral elements. We then

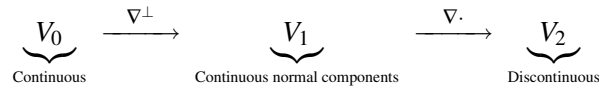
<sup>3</sup>Here sup is short for *supremum*, which is the maximum value, roughly speaking.

<sup>4</sup>The construction here can be extended to the surface of a sphere, or in fact any two-dimensional manifold embedded into  $\mathbb{R}^3$ . For details see [Rognes et al. \(2014\)](#).

obtain compatible finite element methods by choosing a sequence of three finite element spaces,  $(V_0, V_1, V_2)$ , such that:

1.  $V_0$  contains scalar-valued, continuous functions, satisfying periodic boundary conditions.
2.  $V_1$  contains vector-valued functions  $u$ , satisfying periodic boundary conditions, with  $u \cdot n$  continuous across element edges, where  $n$  is the normal to the boundary between two neighbouring elements. The tangential component need not be continuous. This is sufficient continuity for  $\nabla \cdot u$  to be defined globally.
3.  $V_2$  contains scalar-valued functions that may be discontinuous across element boundaries.
4. If  $\psi \in V_0$  then  $\nabla^\perp \psi = (-\psi_y, \psi_x) \in V_1$ .
5. If  $u \in V_1$  with  $\nabla \cdot u = 0$  and  $\int_\Omega u dx = 0$ , then there exists some  $\psi \in V_0$  with  $u = \nabla^\perp \psi$ .
6. If  $u \in V_1$  then  $\nabla \cdot u \in V_2$ .
7. If  $D \in V_2$  with  $\int_\Omega D dx = 0$  then there exists some  $u \in V_1$  with  $\nabla \cdot u = D$ .

We represent this structure in the following diagram.



One example of compatible finite element spaces is  $V_0 = \text{CG2}$ ,  $V_1 = \text{BDM1}$ ,  $V_2 = \text{DG0}$  on triangles. The finite element space BDM1 contains vector-valued functions that have linear  $x$ - and  $y$ -components in each element, with continuous normal components across element boundaries. These finite element spaces are illustrated in Figure 2. If  $\psi \in \text{CG1}$ , then  $\psi$  is continuous and the gradient can be uniformly evaluated. Since  $\psi$  is continuous, the value of  $\psi$  is the same along both sides of each boundary between two elements. This means that the component of  $\nabla \psi$  tangential to the boundary is continuous. The component of  $\nabla \psi$  in the direction normal to the boundary may jump. Transforming  $\nabla \psi$  to  $\nabla^\perp \psi$  rotates the vector by 90 degrees, and so  $\nabla^\perp \psi$  has continuous normal component but possibly discontinuous tangential component. Furthermore, if  $\psi$  is a quadratic polynomial within each element, then  $\nabla \psi$  is linear. Hence, we conclude that  $\nabla^\perp \psi \in \text{BDM1}$ , confirming property 4 above. Similar reasoning by this type of inspection confirms the remaining properties 5-7.

There is a whole range of compatible finite element spaces that satisfy properties 1-7. A particular choice generally depends on: (i) what shape of elements we want, (ii) what relative size of the dimensions of  $V_0$ ,  $V_1$ , and  $V_2$  we want, and (iii) what order of accuracy we want (which depends on the degree of the polynomials used). In Cotter and Shipton (2012), it was shown that  $\dim(V_1) = 2 \dim(V_2)$  (in the case of periodic boundary conditions) is a desirable property. If  $\dim(V_1) < 2 \dim(V_2)$  then there are spurious inertia-gravity waves which are known to cause serious problems in simulating balanced flow Danilov (2010). If  $\dim(V_1) > 2 \dim(V_2)$  then there are spurious Rossby waves, the nature of which is somewhat less clear. On triangles, Cotter and Shipton (2012) identified the following choice as satisfying  $\dim(V_1) = 2 \dim(V_2)$ :  $V_0 = \text{CG2} + \text{B3}$  (continuous quadratic functions plus a cubic ‘‘bubble’’ function that vanishes on element boundaries),  $V_1 = \text{BDFM1}$  (quadratic vector-valued functions that are constrained to have linear normal components along each triangle edge, with continuous normal components), and  $V_2 = \text{DG1}$ . This choice is illustrated in Figure 3. On quadrilaterals, Cotter and Shipton (2012) identified the same property in the choice  $(V_0, V_1, V_2) = (\text{CG1}, \text{RT0}, \text{DG0})$ , and the higher-order extensions  $(\text{CG}(p), \text{RT}(p-1), \text{DG}(p-1))$ . The first two sets of spaces in this family are defined and illustrated in Figure 4.

In this discussion and the accompanying figures, we have defined the finite element spaces on equilateral triangles or on squares. To define them on nonsymmetric triangles/squares, including curved elements to

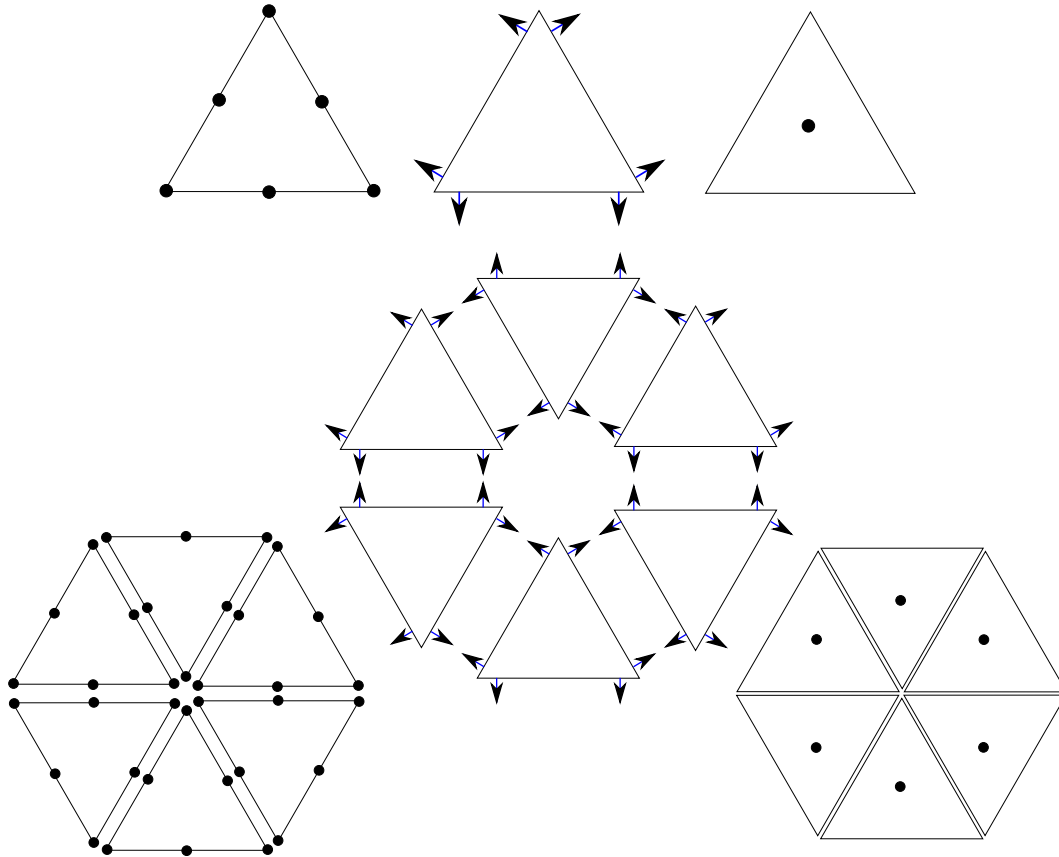


Figure 2: **Top:** Diagrams illustrating  $V_0 = \text{CG2}$  (left),  $V_1 = \text{BDM1}$  (middle),  $V_2 = \text{DG0}$  (right), on triangles. These diagrams show the node points, depicted as circular dots, for a nodal basis for each finite element space on one triangle. Each basis function in the nodal basis is equal to 1 on one node point, and 0 on all other node points, and vary continuously in between (since the basis functions are polynomials within one element). There is one basis function per node point, and the basis coefficient corresponding to that basis function is the value of the finite element function at that node. In the case of  $V_1$ , the basis functions are vector-valued, and each node point has a unit vector associated with it, indicated by an arrow. Each basis function dotted with the unit vector is equal to 1 on one node point, and 0 at all the other nodes. The basis coefficient corresponding to that basis function is the value of the finite element function dotted with the unit vector at that node. **Bottom:** Diagrams illustrating the continuity of functions between several neighbouring elements. Shared node points on adjoining elements mean that a single basis coefficient is used for these nodes. This leads to full continuity between elements for CG2 functions, continuity in the normal components between elements for BDM1 (since only the normal components of vectors are shared), and no implied continuity for DG0.



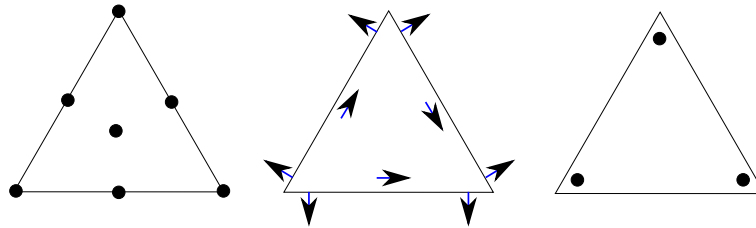


Figure 3: Diagrams illustrating CG2 + B3 (left), BDFM1 (middle), DG1 (right), on triangles. CG2 + B3 is an enrichment of CG2, illustrated in Figure 2, adding the cubic function which vanishes on the boundary of the triangle. BDFM1 is an enrichment of BDM1 to include quadratic vector-valued functions that have vanishing normal components on the boundary of the triangle (there are three of these). The extra degrees of freedom are tangential components on the edge centres. Since tangential components are not required to be continuous, these values are not shared by neighbouring elements and there will be one tangential component node on each side of each edge. BDFM1 has 9 nodes in each element, but 6 of these are shared with other elements, so  $\dim(\text{BDFM1}) = 6N_e$  on the periodic plane. DG1 has 3 nodes in each element, none of which are shared, so  $\dim(\text{DG1}) = 3N_e$ , and hence  $\dim(\text{BDFM1}) = 2\dim(\text{DG1})$  as required.

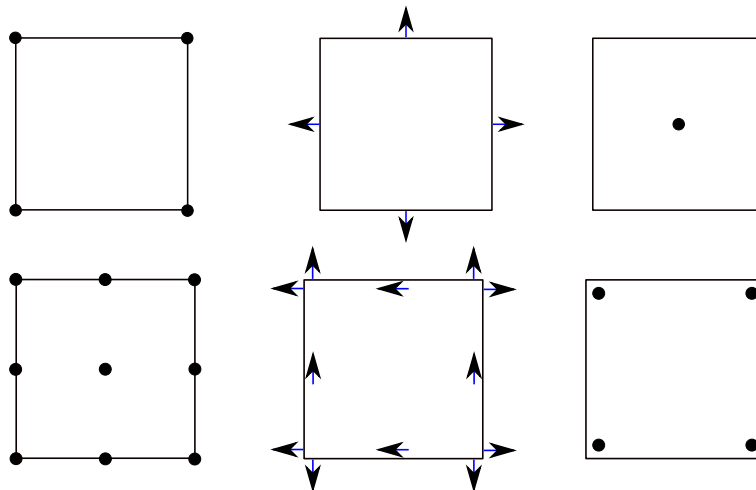


Figure 4: **Top:** Diagram illustrating  $V_0 = \text{CG1}$ ,  $V_1 = \text{RT0}$ ,  $V_2 = \text{DG0}$ , on quadrilaterals. On squares, CG1 means bilinear, i.e. linear function of  $x$  multiplied by linear function of  $y$ . RT0 functions are vector-valued, with the  $x$ -component being linear in  $x$  and constant in  $y$ , and the  $y$ -component being constant in  $y$  and linear in  $x$ . **Bottom:** Diagram illustrating  $V_0 = \text{CG2}$ ,  $V_1 = \text{RT1}$ ,  $V_2 = \text{DG1}$ , where CG2 are biquadratic functions (product of quadratic function of  $x$  and quadratic function of  $y$ ), RT1 have  $x$ -component quadratic in  $x$  and linear in  $y$ , and  $y$ -component linear in  $x$  and quadratic in  $y$ .

approximate the surface of a sphere, we apply geometric transformations to the basis functions defined in the regular case. In the case of  $V_1$ , special transformations (known as Piola transformations) are required that preserve the normal components of the vector-valued function on element boundaries and, in the case of curved elements in three dimensions, keeps the vectors tangential to the surface element. For details of these transformations, together with their efficient implementation, see [Rognes et al. \(2009, 2014\)](#).

We now use these finite element spaces to the linear rotating shallow water equations on the  $f$ -plane, explaining along the way why we consider the compatible finite element method to be an extension of the C-grid finite difference method. The model equations are

$$u_t + fu^\perp + g\nabla h = 0, \quad (14)$$

$$h_t + H\nabla \cdot u = 0, \quad (15)$$

where  $u$  is the horizontal velocity,  $h$  is the layer depth,  $f$  is the (constant) Coriolis parameter,  $g$  is the acceleration due to gravity,  $H$  is the (constant) mean layer depth, and  $u^\perp = (-u_2, u_1)$ .

For our finite element approximation, we choose  $u \in V_1$  and  $h \in V_2$ . Extending the methodology of the previous section (*i.e.* multiplying Equation (14) by a test function  $w \in V_1$ , integrating the pressure gradient term by parts (the boundary term vanishes due to the periodic boundary conditions), multiplying Equation (15) by a test function  $\phi \in V_2$ , and integrating both equations over the domain  $\Omega$ ), we obtain

$$\int_{\Omega} w \cdot u_t \, dx + \int_{\Omega} fw \cdot u^\perp \, dx - \int_{\Omega} g\nabla \cdot w\nabla h \, dx = 0, \quad \forall w \in V_1, \quad (16)$$

$$\int_{\Omega} \phi (h_t + H\nabla \cdot u) \, dx = 0, \quad \forall \phi \in V_2. \quad (17)$$

Since  $h_t + H\nabla \cdot u \in V_2$ , the projection of Equation (15) is trivial, *i.e.* Equation (15) is satisfied exactly under this discretisation. This means that we only need to scrutinise the discretisation of the Coriolis and the pressure gradient terms. In the previous section, we discussed the inf-sup condition for one dimensional compatible finite element methods. The equivalent condition in the two dimensional (and in fact, three dimensional) case is

$$\sup_{w \in V_1} \frac{|\int_{\Omega} \nabla \cdot wh \, dx|}{\|\nabla \cdot w\|_{L^2}} \geq C \|h\|_{L^2}, \quad (18)$$

for all non-constant  $h \in V_2$ . In the compatible finite element case we again obtain  $C = 1$ , and can provably avoid spurious pressure modes.

Regarding the Coriolis term, the crucial condition for large scale balanced flow (*i.e.*, large scale numerical weather prediction) is that the numerical discretisation supports exact geostrophic balance. In the model equations (14-15), if  $\nabla \cdot u = 0$  and  $\int_{\Omega} u \, dx = 0$ , then (15) implies that  $h_t = 0$ . We have  $u = \nabla^\perp \psi$  for some streamfunction  $\psi$ . If we choose  $gh = f\psi$  then

$$u_t = -fu^\perp - g\nabla h = \nabla(f\psi - gh) = 0, \quad (19)$$

and we have a steady state, which we call *geostrophic balance*. If we allow  $f$  to vary with  $y$ , leading to Rossby waves, or introduce nonlinear terms, then this state of geostrophic balance starts to evolve on a slow timescale relative to the rapidly oscillating gravity waves. In large scale flow, the weather system stays close to this balanced state. If we wish to predict the long time evolution of this state accurately, it is essential that the numerical discretisation exactly reproduces steady geostrophic states, otherwise the errors in representing this balance will lead to spurious motions that are much larger than the slow evolution when Rossby waves or nonlinear evolution are introduced, and the forecast will be useless. The C-grid staggering exactly reproduces steady geostrophic states, if the Coriolis term is represented correctly (see [Thuburn et al. \(2009\)](#); [Thuburn and Cotter \(2012\)](#) for how to do this on very general grids); this accounts for the popularity and success of the C-grid in numerical weather prediction.

We now demonstrate that compatible finite element methods also have steady geostrophic states under the same conditions (this was first shown in Cotter and Shipton (2012)). If  $\nabla \cdot u = 0$  and  $\int_{\Omega} u dx = 0$  for  $u \in V_1$ , then  $h_t = -H\nabla \cdot u = 0$ . Next, we can find  $\psi \in V_0$  with  $u = \nabla^{\perp} \psi$ . Then we solve for  $h \in V_2$  from the equation

$$\int_{\Omega} \phi gh dx = \int_{\Omega} \phi f \psi dx, \quad \forall \phi \in V_2, \quad (20)$$

i.e.,  $gh$  is the projection of  $f\psi$  into  $V_2$ . Then

$$\begin{aligned} \int_{\Omega} w \cdot u_t dx &= - \int_{\Omega} fw \cdot u^{\perp} dx + \int_{\Omega} \nabla \cdot wgh dx, \\ &= \int_{\Omega} fw \cdot \nabla \psi dx + \int_{\Omega} \nabla \cdot wgh dx, \\ &= - \int_{\Omega} \nabla \cdot wf \psi dx + \int_{\Omega} \nabla \cdot wgh dx, \\ &= 0, \end{aligned}$$

where we may integrate by parts in the third line since  $w$  has continuous normal component and  $\psi$  is continuous which means that the integration by parts is exact, and where we note in the fourth line that  $\nabla \cdot w \in V_2$ , and so we may use Equation (20) with  $\phi = \nabla \cdot w$ , meaning that we obtain 0 in the final line. Hence, we have an exact steady state.

The extension to the nonlinear shallow water equations makes use of the *vector invariant form*,

$$u_t + qhu^{\perp} + \nabla \left( gh + \frac{1}{2}|u|^2 \right) = 0, \quad (21)$$

$$h_t + \nabla \cdot (hu) = 0, \quad (22)$$

where  $q$  is the shallow water potential vorticity

$$q = \frac{\nabla^{\perp} \cdot u + f}{h}, \quad \nabla^{\perp} \cdot u = -\frac{\partial u_1}{\partial y} + \frac{\partial u_2}{\partial x}, \quad (23)$$

and we have used the split  $(u \cdot \nabla)u = qu^{\perp} + \nabla(|u|^2/2)$ . If we apply  $\nabla^{\perp}$  to Equation (21) and substitute Equation (23) we obtain

$$(qh)_t + \nabla \cdot (qhu) = 0, \quad (24)$$

which is the conservation law for  $q$ . This takes an important role in predicting the large scale balanced flow.

Three issues need to be addressed when discretising these equations with compatible finite element methods. First, if  $u \in V_1$  and  $h \in V_2$ , then  $gh + |u|^2/2$  has discontinuities and the gradient is not globally defined. Second, although we can evaluate  $\nabla \cdot u$  globally, we cannot evaluate  $\nabla \cdot (hu)$  globally, as  $h$  is discontinuous. Third, we need a way of calculating  $q$ . The first issue is addressed by using integration by parts, as in the linear case. The second issue can be addressed by projecting  $uh$  into  $V_1$ , i.e. solving for  $F \in V_1$  such that

$$\int_{\Omega} w \cdot F dx = \int_{\Omega} w \cdot hu dx, \quad \forall w \in V_1. \quad (25)$$

To calculate  $q$ , we need to integrate the  $\nabla^{\perp} \cdot$  operator on  $u$  by parts, since  $u \in V_1$  has insufficient continuity for  $\nabla^{\perp} \cdot u$  to be globally defined. We choose  $\gamma \in V_0$ , and multiply Equation (23) by  $h$ , then  $\gamma \in V_0$ , then finally integrate, to obtain

$$\int_{\Omega} \gamma qh dx = - \int_{\Omega} \nabla^{\perp} \cdot \gamma u dx + \int_{\Omega} \gamma f dx, \quad \forall \gamma \in V_0. \quad (26)$$

If  $h$  is known, then this equation can be solved for  $q \in V_0$  (the factor of  $h$  just reweights the integral in each element).

Having addressed these three issues, we can write down the compatible finite element discretisation of the nonlinear shallow water equations:

$$\int_{\Omega} w \cdot u_t \, dx + \int_{\Omega} w \cdot qF^{\perp} \, dx + \int_{\Omega} \nabla \cdot w \left( gh + \frac{1}{2}|u|^2 \right) \, dx = 0, \quad (27)$$

$$\int_{\Omega} \phi (h_t + \nabla \cdot F) \, dx = 0, \quad (28)$$

where  $F$  and  $q$  are defined from Equations (25) and (26) respectively. There are a number of things to observe about these equations. Firstly, the following quantities are conserved:

$$\text{Mass:} \quad \int_{\Omega} h \, dx, \quad (29)$$

$$\text{Energy:} \quad \int_{\Omega} \frac{h}{2} (|u|^2 + gh) \, dx, \quad (30)$$

$$\text{Total vorticity:} \quad \int_{\Omega} qh \, dx, \quad (31)$$

$$\text{Enstrophy:} \quad \int_{\Omega} q^2 h \, dx. \quad (32)$$

To see that mass is conserved, just take  $\phi = 1$  in Equation (28), and the divergence integrates to 0 by the Divergence Theorem. To see that the total vorticity is conserved, take  $\gamma = 1$  in Equation (26). The  $u$  term vanishes since  $\nabla^{\perp} \gamma = 0$ , and  $f$  is independent of time. Similar direct computations lead to conservation of energy and enstrophy; these make use of the integral formulation and the compatibility properties and are presented in [McRae and Cotter \(pear\)](#) together with numerical verifications of the conservation properties.

It is also interesting to ask what equation  $q$  satisfies in the discrete setting. Our prognostic variables are  $u$  and  $h$ , with  $q$  being purely diagnostic, so we have to make use of the  $u$  and  $h$  equations to obtain the dynamical equation for  $q$ . To do this, we apply a time derivative to Equation (26), and obtain

$$\int_{\Omega} \gamma(qh)_t \, dx + \int_{\Omega} \nabla^{\perp} \gamma \cdot u_t \, dx = 0, \quad \forall \gamma \in V_0. \quad (33)$$

Since  $\nabla^{\perp} \gamma \in V_1$ , we can substitute  $w = \nabla^{\perp} \gamma$  in Equation (27), and we get

$$\int_{\Omega} \nabla^{\perp} \gamma \cdot u_t \, dx = - \int_{\Omega} \nabla^{\perp} \gamma \cdot qF^{\perp} \, dx - \int_{\Omega} \underbrace{\nabla \cdot \nabla^{\perp} \gamma}_{=0} (|u|^2 + gh) \, dx, \quad (34)$$

$$= - \int_{\Omega} \nabla \gamma \cdot qF \, dx, \quad (35)$$

and hence

$$\int_{\Omega} \gamma(qh)_t \, dx - \int_{\Omega} \nabla \gamma \cdot Fq \, dx = 0, \quad \forall \gamma \in V_0. \quad (36)$$

Finally, since  $F$  has continuous normal components and  $\gamma$  is continuous, we may integrate by parts without changing the finite element discretisation, and we obtain

$$\int_{\Omega} \gamma((qh)_t + \nabla \cdot Fq) \, dx = 0, \quad \forall \gamma \in V_0. \quad (37)$$

This is the projection of Equation (24) into  $V_0$ , and so the discretisation has a consistent potential vorticity conservation law.

It should be noted that for shallow water equations in the geostrophic limit, it is desirable to dissipate enstrophy at the grid scale rather than conserve it exactly, due to the enstrophy cascade to small scales which would otherwise cause gridscale oscillations. In [McRae and Cotter \(pear\)](#), (27) was modified

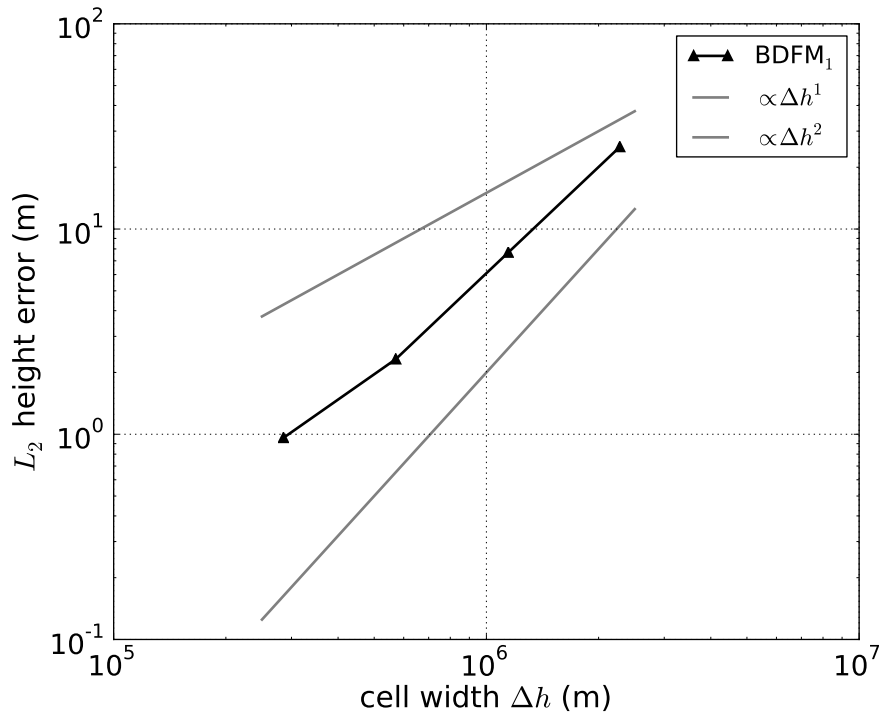


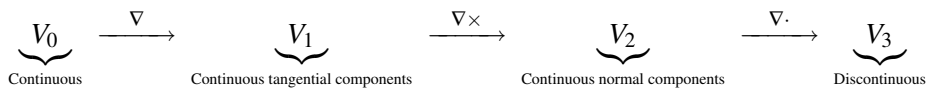
Figure 5:  $\|h - h_{\text{ref}}\|$  versus mesh size (where  $h_{\text{ref}}$  is a reference solution and  $h$  is the numerical solution) for the Williamson 5 test case.  $\Delta t = 225\text{s}$ , 4 quasi-Newton iterations per time step.

to dissipate enstrophy at the gridscale whilst conserving energy; this follows the Anticipated Potential Vorticity Method strategy of Arakawa and Hsu (1990). It was shown in McRae and Cotter (pear) that this modification leads to stable vortex merger solutions that do not develop gridscale oscillations. Further, it is desirable to replace APVM by stable, accurate upwind advection schemes for  $q$  and  $h$ ; we are developing the integration of discontinuous Galerkin methods for  $h$  and higher-order Taylor-Galerkin methods for  $q$  in current work.

Finally, we present some results integrating the shallow water equations on the sphere using Test Case 5 (the mountain test case) as specified in Williamson et al. (1992). Figure 5 gives a convergence plot upon comparing the height field with the solution from a resolved pseudospectral calculation, using the BDFM1 space with a successively refined icosahedral mesh. The expected 2nd order convergence is obtained. Figure 6 is an image of the velocity and height fields at day 15, while Figure 7 shows the evolution of the potential vorticity field out to 50 days.

## 4 Outlook on applications in three dimensional models

Current work as part of the UK GungHo dynamical core project is investigating the application of compatible finite element spaces to three dimensional compressible flow. In three dimensions, we now have four finite element spaces, and the required structure is depicted in the following diagram



where  $V_1$  and  $V_2$  are both vector-valued finite element spaces. There is also an extension of the vector invariant form into three dimensions. We choose  $u \in V_2$ ,  $\rho \in V_3$ , and it is possible to define a vorticity

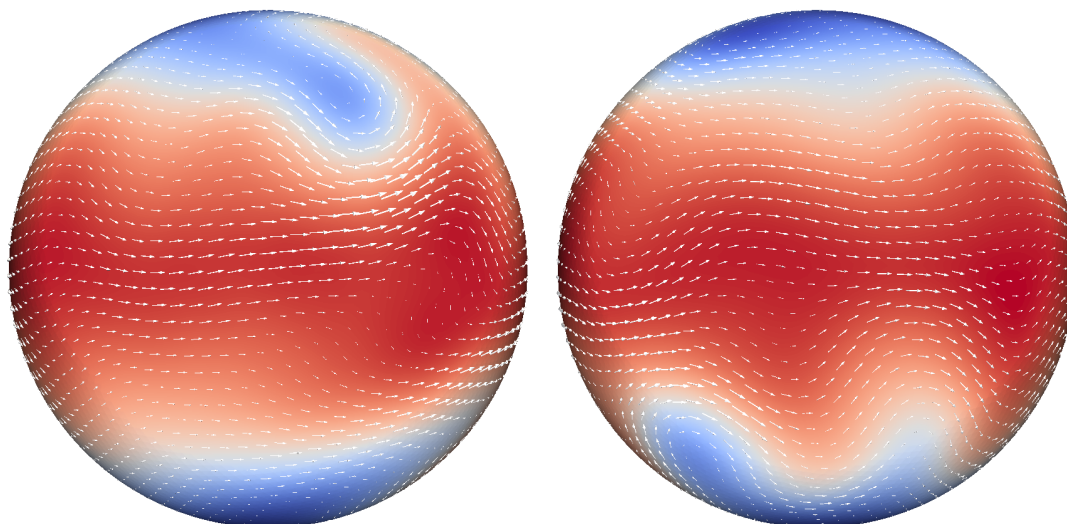
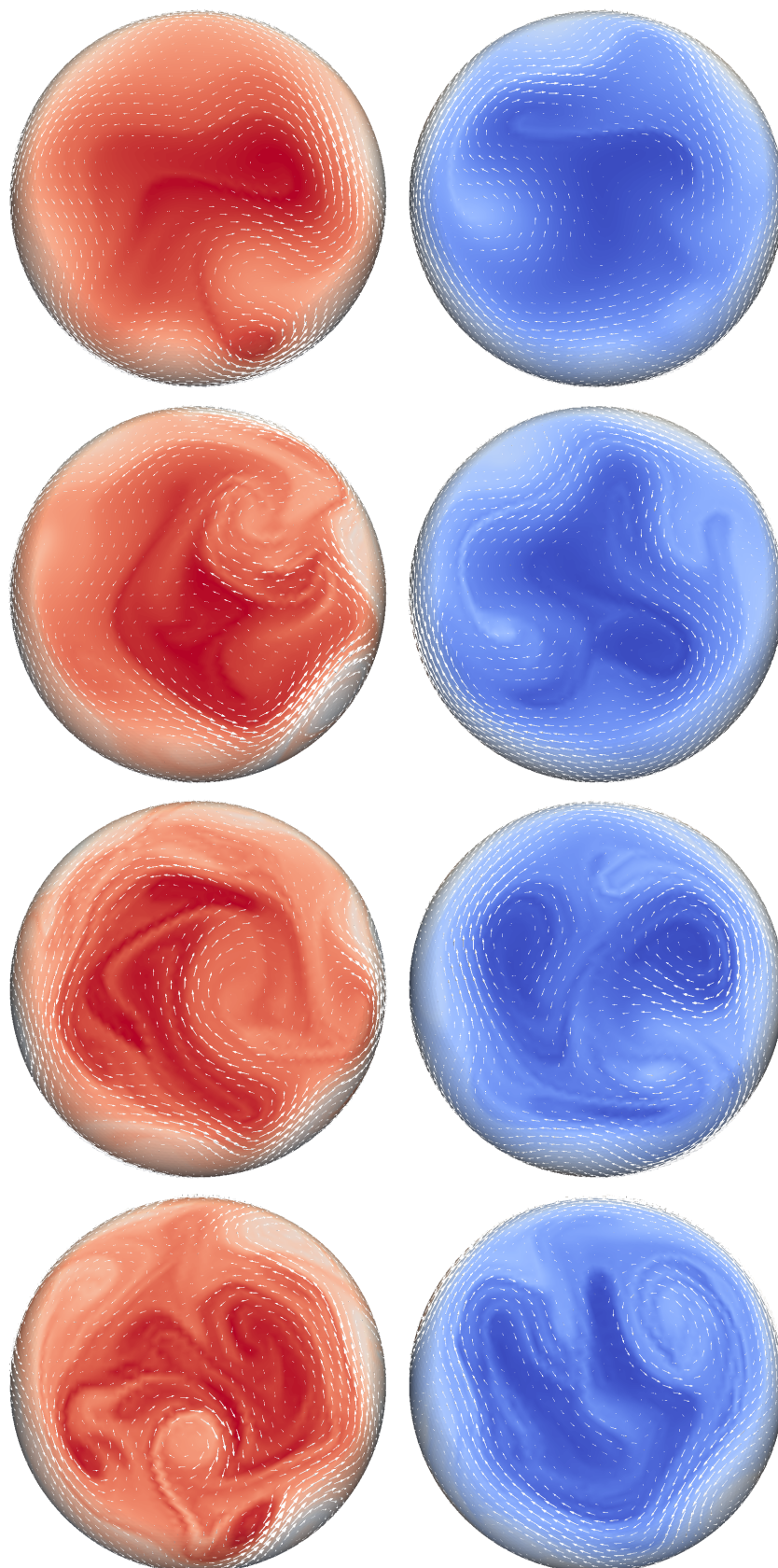


Figure 6: Snapshots of the velocity and height fields in the Williamson 5 test case at 15 days. Blue represents small fluid depth, red represents large fluid depth. Left: facing the mountain. Right: reverse side.

$\omega \in V_1$  using integration by parts. For a vertical discretisation similar to the Lorenz grid, we could choose potential temperature  $\theta$  to be in  $V_3$ , however the extension of the Charney-Phillips grid would require  $\theta$  to be in the vertical part of  $V_2$ ; this is the subject of current work. Other challenges in this setting include determining the correct form of the pressure gradient term, the treatment of the velocity advection (which would be *via* an implied vorticity equation), and the efficient solution of the coupled linear system that is required for a semi-implicit implementation.

## References

- Allen, M. B., R. E. Ewing, and J. Koebe (1985). Mixed finite element methods for computing groundwater velocities. *Numerical Methods for Partial Differential Equations 1*(3), 195–207.
- Arakawa, A. and Y.-J. G. Hsu (1990). Energy conserving and potential-enzstrophy dissipating schemes for the shallow water equations. *Monthly Weather Review 118*(10), 1960–1969.
- Arakawa, A. and V. Lamb (1981). A potential enstrophy and energy conserving scheme for the shallow water equations. *Monthly Weather Review 109*(1), 18–36.
- Arnold, D., R. Falk, and R. Winther (2006). Finite element exterior calculus, homological techniques, and applications. *Acta Numerica 15*, 1–155.
- Arnold, D., R. Falk, and R. Winther (2010). Finite element exterior calculus: from Hodge theory to numerical stability. *Bull. Amer. Math. Soc.(NS) 47*(2), 281–354.
- Auricchio, F., F. Brezzi, and C. Lovadina (2004). *Mixed Finite Element Methods*, Volume 1, Chapter 9. Wiley.
- Boffi, D., F. Brezzi, and M. Fortin (2013). *Mixed finite element methods and applications*. Springer.
- Bossavit, A. (1988). Whitney forms: a class of finite elements for three-dimensional computations in electromagnetism. *IEE Proceedings A (Physical Science, Measurement and Instrumentation, Management and Education, Reviews) 135*(8), 493–500.



*Figure 7: Top to bottom: snapshots of the potential vorticity field in the Williamson 5 test case, at 20, 30, 40 and 50 days respectively, with superposed (scaled) velocity vectors. Left: facing North pole. Right: facing South pole.*

- Brezzi, F. and M. Fortin (1991). *Mixed and hybrid finite element methods*. Springer-Verlag New York, Inc.
- Comblen, R., J. Lambrechts, J.-F. Remacle, and V. Legat (2010). Practical evaluation of five partly discontinuous finite element pairs for the non-conservative shallow water equations. *International Journal for Numerical Methods in Fluids* 63(6), 701–724.
- Cotter, C. and D. Ham (2011). Numerical wave propagation for the triangular P1DG-P2 finite element pair. *Journal of Computational Physics* 230(8), 2806 – 2820.
- Cotter, C. and J. Shipton (2012). Mixed finite elements for numerical weather prediction. *Journal of Computational Physics* 231(21), 7076–7091.
- Cotter, C. and J. Thuburn (2014). A finite element exterior calculus framework for the rotating shallow-water equations. *J. Comp. Phys.* 257, 1506–1526.
- Cotter, C. J., D. A. Ham, and C. C. Pain (2009). A mixed discontinuous/continuous finite element pair for shallow-water ocean modelling. *Ocean Modelling* 26, 86–90.
- Danilov, S. (2010). On utility of triangular C-grid type discretization for numerical modeling of large-scale ocean flows. *Ocean Dynamics* 60(6), 1361–1369.
- Hiptmair, R. (2002). Finite elements in computational electromagnetism. *Acta Numerica* 11(0), 237–339.
- Karniadakis, G. E. M. and S. Sherwin (2005). *Spectral/hp Element Methods for Computational Fluid Dynamics*. Oxford Science Publications.
- Le Roux, D. Y. (2012). Spurious inertial oscillations in shallow-water models. *Journal of Computational Physics* 231(24), 7959–7987.
- Le Roux, D. Y. and B. Pouliot (2008). Analysis of numerically induced oscillations in two-dimensional finite-element shallow-water models Part II: Free planetary waves. *SIAM Journal on Scientific Computing* 30(4), 1971–1991.
- Le Roux, D. Y., V. Rostand, and B. Pouliot (2007). Analysis of numerically induced oscillations in 2D finite-element shallow-water models Part I: Inertia-gravity waves. *SIAM Journal on Scientific Computing* 29(1), 331–360.
- Le Roux, D. Y., A. Sène, V. Rostand, and E. Hanert (2005). On some spurious mode issues in shallow-water models using a linear algebra approach. *Ocean Modelling*, 83–94.
- McRae, A. and C. Cotter (to appear). Energy- and enstrophy-conserving schemes for the shallow-water equations, based on mimetic finite elements. *QJRMSS*. Preprint at <http://arxiv.org/abs/1305.4477>.
- Ringler, T. D., J. Thuburn, J. B. Klemp, and W. C. Skamarock (2010). A unified approach to energy conservation and potential vorticity dynamics for arbitrarily-structured C-grids. *Journal of Computational Physics* 229(9), 3065–3090.
- Rognes, M., D. Ham, C. Cotter, and A. McRae (2014). Automating the solution of PDEs on the sphere and other manifolds. to appear in *Geosci. Model Dev.*
- Rognes, M., R. Kirby, and A. Logg (2009). Efficient assembly of  $H(\text{div})$  and  $H(\text{curl})$  conforming finite elements. *SISC* 31(6), 4130–4151.



- Rostand, V. and D. Le Roux (2008). Raviart–Thomas and Brezzi–Douglas–Marini finite-element approximations of the shallow-water equations. *International journal for numerical methods in fluids* 57(8), 951–976.
- Staniforth, A. and J. Thuburn (2012). Horizontal grids for global weather and climate prediction models: a review. *Q. J. Roy. Met. Soc* 138(662A), 1–26.
- Thuburn, J. (2008). Numerical wave propagation on the hexagonal C-grid. *J. Comp. Phys.* 227(11), 5836–5858.
- Thuburn, J. and C. Cotter (2012). A framework for mimetic discretization of the rotating shallow-water equations on arbitrary polygonal grids. *SIAM J. Sci. Comp.*.
- Thuburn, J., T. D. Ringler, W. C. Skamarock, and J. B. Klemp (2009). Numerical representation of geostrophic modes on arbitrarily structured C-grids. *J. Comput. Phys.* 228, 8321–8335.
- Walters, R. and V. Casulli (1998). A robust, finite element model for hydrostatic surface water flows. *Communications in Numerical Methods in Engineering* 14, 931–940.
- Wathen, A. (1987). Realistic eigenvalue bounds for the Galerkin mass matrix. *IMA Journal of Numerical Analysis* 7(4), 449–457.
- Williamson, D. L., J. B. Drake, J. J. Hack, R. Jakob, and P. N. Swarztrauber (1992). A standard test set for numerical approximations to the shallow water equations in spherical geometry. *Journal of Computational Physics* 102(1), 211–224.

